CircSLC8A1 inhibits sunitinib resistance in renal cell carcinoma by promoting the ubiquitination and degradation of FUS

Linhui Wang (wanglinhui@smmu.edu.cn)
Department of Urology, Changhai Hospital, Naval Medical University
Jie Wang
Department of Urology, Changhai Hospital, Naval Medical University
Xinxin Gan
Department of Urology, Changhai Hospital, Naval Medical University
Qiong Chen
Department of Urology, Changhai Hospital, Naval Medical University
Bing Liu
Department of Urology, Eastern Hepatobiliary Surgery Hospital, Navy Military Medical University
Sujuan Zheng
Department of Laboratory Diagnostics, Changhai Hospital, Navy Medical University
Yi Bao
Department of Urology, Changzheng Hospital, Naval Medical University
Anbang Wang
Department of Urology, Changzheng Hospital, Naval Medical University
Rui Yan
Department of Urology, Changhai Hospital, Naval Medical University
Yewei Bao
Department of Urology, Changhai Hospital, Naval Medical University
Wenliang Gong
Department of Urology, Changhai Hospital, Naval Medical University
Yuexiang Wang
CAS Key Laboratory of Tissue Microenvironment and Tumor, Shanghai Institute of Nutrition and Health, University of Chinese Academy of Sciences
Fu Yang
Department of Medical Genetics, Navy Military Medical University

Research Article

Keywords: Renal cell carcinoma, Circular RNAs, SLC8A1, FUS, Targeted drug, Resistance

Posted Date: February 17th, 2022

DOI: https://doi.org/10.21203/rs.3.rs-1360067/v1

Abstract

Background:

Circular RNAs play an important role in many biological processes, including tumor occurrence and development. Targeted drug such as sunitinib is currently the first-line therapy for the treatment of metastatic renal cell carcinoma. Drug resistance is an important problem faced by clinicians. Currently, the role and underlying molecular mechanisms of circular RNAs in targeted drug resistance for renal cell carcinoma remain unknown.

Methods:

We generated the sunitinib-resistant renal cell carcinoma (RCC) cell lines Sun-7R and Sun-AR. Then, we used RNA sequencing (RNA-Seq) to identify the circular RNA related to targeted drug resistance in RCC, cSLC8A1. qRT-PCR was used to detect the expression of circRNAs、mRNAs in human tissues and cells. The actinomycin D experiment, RNase R digestion experiment, and fluorescence in situ hybridization (FISH) experiment were performed to verify the circularity characteristics of cSLC8A1. CCK-8 experiment and plate clone experiment were performed to verify the reactivity of RCC cells to sunitinib. The effects of circSLC8A1 on RCC cells were explored by transfecting with knockdown and over-expressed lentivirus in vitro and in vivo. Western-blot and immunohistochemical experiment were used to analyze the protein expression level of FUS.

Results:

We verified that cSLC8A1 was expressed at low levels in sunitinib-resistant tissues and cell lines、and cSLC8A1 expression was associated with response to sunitinib in RCC patients . Overexpression of cSLC8A1 inhibited cell proliferation and migration, thereby increasing the sensitivity of renal cell carcinoma cells to sunitinib. We found a novel function and mechanism of circRNAs that cSLC8A1 promotes the ubiquitination and degradation of the FUS protein and then mediates the drug resistance process.

Conclusions:

cSLC8A1 inhibits resistance by promoting the ubiquitination and degradation of the FUS protein. cSLC8A1 plays an important role in drug resistance and is expected to become a target for reversing sunitinib resistance in RCC.

Background

Renal cell carcinoma (RCC) is one of most common malignant tumor of the urinary system[1, 2]. Approximately 30% of patients present with metastatic disease when first visit; and one-third of patients who are treated for localized RCC with curative intent have a relapse in distant sites[3]. The cell of RCC is not sensitive to radiotherapy and chemotherapy; thus, the main common treatment methods after

metastasis including targeted therapy or immune-checkpoint inhibitors[4]. Although targeted TKIs such as sunitinib have been the first-line treatment for patients with metastasis throughout the past ten years, one-third of patients develop resistance in the early stage of drug treatment[5]. In addition, patients who are sensitive to initial treatment will also face the problem of secondary drug resistance[6]. The molecular mechanisms related to targeted drugs resistance for RCC patients are still unclear. Studying the relevant mechanisms and identifying new therapeutic targets to reverse drug resistance will expand the application prospects of targeted drug therapy for patients with metastatic RCC.

Recent studies have shown that mammals express a large amount of circular RNAs (circRNAs). CircRNAs are mainly products of backsplicing events, in which exons are joined to the upstream exon instead of downstream exons, thus forming a covalently closed circRNA[7] . These circRNAs are usually tissue-specific and are related to the development during a specific period. An increasing number of studies have shown that circRNAs play an important role in many biological processes, including tumor occurrence and development[8-11]. Most circRNAs are exported to the cytoplasm after formation, acting as miRNA sponges, binding with RBPs, or encoding proteins[12]. The biological functions of circRNAs in target drug resistance of RCC remain largely unknown and require further research.

In this study, we used RNA sequencing (RNA-Seq) to explore the circRNAs associated with sunitinib resistance in RCC, and we found that circSLC8A1 (cSLC8A1) showed low expression in resistant tissues and cells. A novel function and mechanism of cSLC8A1 were explored in this study.

Methods

Tissues.

All tissue specimens were obtained from the Kidney Cancer Specimen Bank of the Department of Urology, Shanghai Changzheng Hospital, and the Urology Specimen Bank of Shanghai Changhai Hospital. The use of all tissue specimens involved in this study was approved by the ethics committee of Changzheng Hospital Affiliated with Naval Military Medical University and Changhai Hospital Affiliated with Naval Military Medical University. From December 2005 to January 2020, primary tumors were obtained after RCC surgery in Changzheng Hospital and the Department of Urology of Changhai Hospital Affiliated with Naval Military Medical University. After the specimens were obtained, they were immediately treated with liquid nitrogen and stored in a -80°C freezer or were fixed with formalin and embedded in paraffin blocks. The specimens were used for PCR, Western blot analysis, tissue chip preparation, and immunohistochemical analysis.

Animal studies.

Female BALB/c nude mice (6-8 weeks old) were purchased from Shanghai Jihui Laboratory Animal Care Co., Ltd. (Shanghai, China) and maintained under specific pathogen-free (SPF) conditions in a controlled

environment of 20-22°C and 50-70% humidity on a 12/12 h light/dark cycle. Food and water were provided ad libitum. Small animal euthanasia equipment was used for animal euthanasia. Mice were put into the euthanasia chamber filled with 99.9% CO2 gas for 10 min. All animal experiments were performed with approval from the Shanghai Medical Experimental Animal Care Committee.

Animal studies were approved by the Institutional Animal Care and Use Committee of the Second Military Medical University, Shanghai, China. A total of 5×10^6 cells of experimental group and control group were injected subcutaneously into the flanks of the mice. When the xenografts grew to 100 mm^3, the mice were treated with sunitinib (40 mg/kg/day). Xenograft volumes were evaluated by caliper measurements of two perpendicular diameters and calculated individually with the following formula: Volume = a×b2/2 (where a represents the length and b represents the width). Xenograft samples were collected for histological evaluation (paraffin sections) or were snap frozen in liquid nitrogen.

Cell lines. All human RCC cell lines (786-O and ACHN) were purchased from the American Type Culture Collection (ATCC). 786-O cells were cultured in RPMI-1640 medium (Gibco) supplemented with 10% FBS. ACHN cells were cultured in DMEM (Gibco) supplemented with 10% FBS. All cells were cultured at 37°C in 5% CO2.

To generate sunitinib-resistant cell lines, we used a low to high concentration gradient of sunitinib to stimulate 786-O and ACHN cells. When the 786-O and ACHN cells were adherent at a confluence of 50%, the culture medium was replaced with medium containing sunitinib at an initial concentration of 2 μM. After culture for 48 h, the medium was replaced with fresh drug-free culture medium, and cells were then passaged after the cell status was restored. After two passages in medium containing each concentration of sunitinib, the concentration was increased by 0.5 μM to the final concentration of 20 μM. The culture was maintained at this concentration. Resistant cells were cryopreserved in serum-free cryopreservation containing 5μM of sunitinib.

RNA-Seq analysis.

RT-PCR and qRT-PCR.

RNA was reverse transcribed using RT SuperMix for qPCR (+gDNA Wiper) (Takara, Japan). SYBR Green Master Mix (Takara, Japan) was used for qRT-PCR. The circRNA and mRNA levels were normalized to the levels of GAPDH. All primer sequences are listed in Supplementary Data 1.

RNA FISH-immunofluorescence.

The probes were designed and synthesized by Genepharma (Shanghai, China) and Cy3-labeled probes were specific to cSLC8A1. The probe sequences : 5’-Cy3-CAACCTAACAATTTCATCATTCTGG. 786-O and ACHN cells were fixed in 4% paraformaldehyde and permeabilized with 0.1% tritonX-100. Subsequently,

hybridization using cSLC8A1 probes was performed at 37°C in the dark overnight, and cells were rinsed in SSC buffer at 42°C. Then, cells were incubated with blocking buffer (PBST containing 5% bovine serum albumin) for 30 min at room temperature. FUS (ab124923, anti-rabbit, 1:200) was performed at 4°C in the dark overnight. Goat anti rabbit IgG FITC conjugated (MultiSciences Biotech) was used as the secondary antibody at 1:500. Subsequently, cells were incubated with DAPI (Vector Laboratories) for 30 min. Images were acquired using a confocal microscope.

RNase R treatment.

Two micrograms of total RNA was incubated for 30 min at 37°C in the absence or presence of 5 U/μg RNase R (Epicentre Technologies, Madison, WI, USA), and the resulting RNA was subsequently purified with an RNeasy MinElute Cleaning Kit (Qiagen) and analyzed by qRT-PCR.

Actinomycin D assays.

786-O, ACHN, Sun-7R and Sun-AR cells were seeded in six-well plates (10^5 cells per well). Twenty-four hours later, the cells were exposed to 2 μg/ml actinomycin D (Abcam) and collected at the indicated time points. RNA stability was analyzed using qRT-PCR, and the values measured in the treatment groups were normalized to the values measured in the mock treatment group (the 0 h group).

Vector construction and cell transduction.

Lentiviruses expressing human cSLC8A1 and FUS were constructed and produced by the Chinese Academy of Sciences (Shanghai). 786-O, ACHN, Sun-7R and Sun-AR cells were transduced following the manufacturer's instructions. After 72 h, puromycin was added to select the stably transduced cell lines.

Cell counting kit 8 (CCK-8) assay.

RCC cells were cultured in medium containing different concentrations of sunitinib (0 μM, 2 μM, 4 μM, 8 μM, 10 μM, 16 μM and 20 μM). Then, 100 μl of culture medium containing 10 μl of CCK-8 reagent (Dojindo Molecular Technologies, Inc., Kumamoto, Japan) was added to each well for another 2 h of incubation at 37°C. The absorbance was measured at 450 nm using a microplate reader (Varioskan Flash; Thermo Scientific, Waltham, MA, USA). Viability (%) was calculated based on the optical density (OD) values. All experiments were independently repeated in triplicate at separate times.

Plate colony formation assay.

RCC cells (500 cells) were seeded into 6-well plates in medium containing sunitinib (5 μM) and cultured in a 37°C incubator for 10 days until most single colonies contained more than 50 cells. The plates were washed with phosphate-buffered saline (PBS), fixed with 4% paraformaldehyde, and stained with crystal violet. The number of colonies containing more than 50 cells was counted in each well.

RNA pulldown assay.

For the RNA pulldown assay, 1×10^7 cells were washed in ice-cold PBS, lysed in 500 μl of coimmunoprecipitation (co-IP) buffer (Thermo Scientific) supplemented with a cocktail of proteinase inhibitors, phosphatase inhibitors, and an RNase inhibitor (Invitrogen). Lysates were then incubated with 3 μg of biotinylated DNA oligo probes targeting the cSLC8A1 backsplice junction region (sense) or the corresponding complementary probes (antisense) for 2 h at room temperature. A total of 50 μl of washed streptavidin C1 magnetic beads (Invitrogen) were added to each binding reaction and further incubated for another hour at room temperature. The beads were washed briefly with co-IP buffer five times. Finally, the retrieved proteins were used for mass spectrometry or western blot analysis. The probe sequences are listed in Supplementary Data 4.

Wound healing assay

RCC cells (5×10^5cells) were seeded into 6-well plates in medium containing sunitinib (5 μM). Then, a wound was made by using a 200 μl pipette tip on the cell monolayer and photographs were taken at the appropriate time to estimate the area occupied by migratory cells.

Transwell assay

Transwell assay was used to evaluate the invasion and migration capacities of RCC cells in vitro. Cells at a concentration of 1×10^4 cells in 500 μl of serum-free medium with containing sunitinib (5 μM) were inoculated in the upper chamber, coated with (invasion assay)or without (migration assay) growth factor reduced Matrigel®, and medium containing 10% FBS was added into the lower chamber as a chemoattractant. After incubation for the appropriate time, cells on the upper surface of the membrane were removed by wiping with a Q-tip, and the invaded or migrated cells were fixed with formaldehyde and stained using 0.5% crystal violet. The numbers of invaded and migrated cells were counted in five randomly selected fields under a microscope.

Mass

RIP.

RIP was performed with a Magna RIP RNA-Binding Protein Immunoprecipitation Kit (Millipore, Billerica, MA, USA) according to the manufacturer's instructions. Coprecipitated RNA was detected by qRT-PCR.

Western blot analysis. Cell lysates or retrieved proteins were analyzed by immunoblotting with primary antibodies and an IRDye 800 CW-conjugated secondary antibody (Rockland Immunochemicals, USA). The fluorescence intensity was determined with an Odyssey fluorescence scanner system (Li-Cor Biosciences, USA). GAPDH was used as the loading control. The other antibodies were as follows: anti-FUS (ab23439, anti-rabbit, 1:1000), anti-Ubiquitin (ab7780, rabbit, 1:1000), and anti-GAPDH (ab9485, rabbit, 1:2500).

Immunohistochemistry.

Specimens were stained with an anti-FUS antibody (ab124923, 1:100). The sections were heated at 70°C for 1 h, dewaxed in xylene, and dehydrated through an alcohol gradient. After antigen retrieval, quenching of endogenous peroxidase activity with 3% H2O2 and blocking of nonspecific binding with normal bovine serum, the sections were incubated with the primary antibody overnight at 4°C. The slides were then incubated with a horseradish peroxidase (HRP)-conjugated secondary antibody for 10 min at 37°C. Finally, staining was visualized with diaminobenzidine (DAB) solution and counterstaining with hematoxylin. Two pathologists blinded to the patient outcomes independently scored the staining intensities and percentages of positive tumor cells.

Co-IP.

To detect protein–protein interactions, cells were lysed in 500 μl of co-IP buffer supplemented with a cocktail of proteinase inhibitors, phosphatase inhibitors, and an RNase inhibitor. The lysates were centrifuged at 12,000 × g for 30 min, and the supernatant was used for immunoprecipitation with beads, which were preincubated with the corresponding antibodies. After incubation at 4°C overnight, the beads were washed three times with co-IP buffer. SDS sample buffer was added to the beads, and the immunoprecipitates were used for western blot analysis.

Clinical data

All patients developed tumor metastasis or recurrence and received regular sunitinib treatment for more than 3 months. The starting point of the follow-up study was the time to receive regular sunitinib treatment, and endpoints included time to disease progression and death. The evaluation criteria for tumor response to drugs were based on Response Evaluation Criteria in Solid Tumors (RECIST). All patients developed tumor metastasis or recurrence and received regular sunitinib treatment for more than 3 months. We divided these patients into sunitinib sensitive group and resistant group according to RECIST1.1. Sensitive group included patients with complete response (CR) or partial response (PR) or

patients with stable disease (SD) maintained for at least 6 months. Resistant group patients experienced progressive disease (PD)[13].

Data analysis.

All statistical analyses in this study were performed with SPSS 16.0 software (SPSS Inc., USA). Data are presented as the mean±s.d. values. The significance of differences between the mean values of two groups was analyzed by two-tailed Student's t-test. Spearman correlation analysis was performed to evaluate correlations between two variables. The Pearson chi-square test was used to analyze the clinical variables. Kaplan–Meier survival analysis was performed, and the survival of ccRCC patients stratified by cSLC8A1 expression was compared by the log-rank test. Cox proportional hazards regression analysis was utilized to analyze the effects of clinical variables on patient survival. P values <0.05 were considered significant.

Data availability.

The gene expression profiles of the generated sunitinib-resistant RCC cell lines have been deposited in GEO with the accession code GSE173572. The mass spectrometry data that support the findings of this study are included in Supplementary Data 4. The authors declare that all other relevant data supporting the findings of this study are available upon request.

Results

Identification of circular RNAs by RNA-seq analysis in sunitinib-resistant RCC cells

To obtain sunitinib-resistant RCC cells, we treated the RCC cell lines 786-O and ACHN with sunitinib and named the resulting cell lines Sun-7R and Sun-AR, respectively (Fig 1A). Compared with the parental RCC cell lines, Sun-7R and Sun-AR exhibited increased resistance to sunitinib, as determined by the increased half-maximal inhibitory concentration (IC50), and formed an increased number of colonies under sunitinib stimulation, indicating a poor response to sunitinib (Fig 1B, C). Through animal drug simulation experiments in vitro, it was confirmed that the drug-resistant cell line we constructed was resistant to sunitinib (Fig 1D).

To identify circRNAs involved in sunitinib resistance in RCC, we conducted Ribo-Zero RNA-Seq (NovelBio Bio-Pharm Technology Co.,Ltd) on Sun-7R and Sun-7C (parental 786-O) cells. The sequencing statistics were described. We detected 24409 circRNAs in total, among which 4673 (19.1%) were highly expressed in both cell lines (FPKM>1) and 3221 were identified in circBase (Fig 2A,B). Furthermore,4065 circRNAs consisted of protein coding exons and the length of most exonic circRNAs was less than 1,000 nucleotides (Fig. 2C). Then, we analyzed the correlations between the expression levels of these circRNAs

and their corresponding mRNAs in the two groups of cells. The expression levels of the circRNAs showed three peaks, and the expression levels of the downregulated circRNAs were far greater than those of the upregulated circRNAs (Fig 2D). The host pathway analysis results indicated that the expression of circRNAs corresponding to drug resistance-related pathways, the VEGF pathway and the PI3K-Akt pathway, was significantly changed (Fig S1A, B). We observed a significant difference (fold change >1, FDR<0.05) in the expression of 35 circRNAs—namely, 18 upregulated and 17 downregulated circRNAs—between the two groups(Fig 2E,Fig S1C, Supplementary Data 3.). Next, we selected the 12 circRNAs (6 upregulated and 6 downregulated) with the largest expression changes for verification (Table S1). We successfully validated these 12 circRNAs in RCC cell lines by reverse transcription–polymerase chain reaction (RT-PCR) using circRNA-specific divergent primers and Sanger sequencing, demonstrating that they were truly circular and not linear (Fig S1D, E, F). We detected the expression of these circRNAs in Sun-7R and Sun-7C cells by quantitative reverse transcription–polymerase chain reaction (qRT-PCR) (Fig 2F). The findings were consistent with the RNA-Seq results.

cSLC8A1 is downregulated in sunitinib-resistant RCC patients and RCC cell lines

We selected cSLC8A1 (circBase ID: hsa_circ_0000994), which is generated from backsplicing of exon 2 of the SLC8A1 gene and has a length of 1832 nt, for further study (Fig 3A). The reasons were as follows:(i) cSLC8A1 was significantly downregulated in Sun-7R and Sun-AR cells compared with the corresponding control cells, although the levels of solute carrier family 8, member 1 (SLC8A1) pre-miRNA (pSLC8A1) and SLC8A1 mRNA (mSLC8A1) did not differ (Fig S1G). This result indicated that the lower expression of cSLC8A1 in RCC was not simply a by-product of splicing and was suggestive of functionality. Then, we determined the levels of cSLC8A1 in five different RCC cell lines. We found that the cell line with higher cSLC8A1 expression (OSRC-2) was more sensitive to sunitinib, whereas the cell line (A498) with lower cSLC8A1 expression was more resistant to sunitinib resistance (Fig 3B, C). This funding revealed that cSLC8A1 is also downregulated in sunitinib primary resistance of RCC. We determined the levels of cSLC8A1 and mSLC8A1 in tumor tissues from 46 patients (Table1). We divided these patients into sunitinib sensitive group and resistant group according to RECIST1.1. RT-PCR showed that the level of cSLC8A1 in resistant tissues was lower than that in sensitive tissues, but there was no significant difference in the mSLC8A1 expression level (Fig 3D). Our results indicated that cSLC8A1 is downregulated in sunitinib-resistant RCC patient tissues and RCC cells.

(ii) The abundance of cSLC8A1 expression in RCC cells was higher than that of linear mSLC8A1. We found that in RCC cell lines or tissues by qRT-PCR, the average Ct value of the GAPDH was about 14, and the average Ct value of cSLC8A1 was 24, but the average Ct value of linear mSLC8A1 was about 32. To verify the relative abundance of cSLC8A1 and linear mSLC8A1 in RCC cells, we designed three different primers (Fig 3A). One was a specific primer for cSLC8A1, the design principle was that the second exon of SLC8A1 was used as a transcription template, and the primer product spanned the splicing site, which could specifically reflect the expression level of cSLC8A1 in cells; The second primer was linear specific

primers for mSLC8A1 designed based on the exons 2, 3, and 4 of SLC8A1 as transcription templates. The primer products were 5’ to 3’directional linear expression of mSLC8A1, which could fully reflect the expression level of its linear mSLC8A1; The third was a public primer designed based on exon 2 of SLC8A1.The product was the direction of 5' to 3', and wouldn’t span the splicing site. The product could reflect the relative expression of both cSLC8A1 and linear mSLC8A1. We named it L/c-SLC8A1. First, we detected the circular characteristics of cSLC8A1 in the 786-O cell line. The RT-PCR results showed that cSLC8A1 was resistant to degradation by RNase R, indicating that cSLC8A1 is circular (Fig 3E). The products of L/c-SLC8A1 still retains most of the circRNA (Fig 3F). We further used random hexamer or oligo (dT)18 primers in reverse transcription, and subsequent RT-PCR analysis showed that cSLC8A1 and L/c-SLC8A1 could be amplified by the random primers but not the oligo(dT)18 primers (Fig 3G). Moreover, we used actinomycin D to inhibit RNA transcription, and measured the levels of cSLC8A1, mSLC8A1 and L/c-SLC8A1 at different time points in 786-0 O cells. The relative level of cSLC8A1 and L/c-SLC8A1 were markedly higher than that of linear mSLC8A1 at 4, 8 and 12 h after actinomycin D treatment (Fig 3H). Nuclear and cytoplasmic fractionation as well as fluorescence in situ hybridization (FISH) revealed that cSLC8A1 was predominantly localized in the cytoplasmic and also nucleus (Fig 3I, J). These results demonstrate that cSLC8A1 is an abundant, circular and stable transcript.

According to the back-splicing mechanism of circular RNA, we analyzed the intron sequences on both sides of exon 2 of the SLC8A1 gene and found that the introns on both sides have longer sequence fragments of 21599 bases (chr2: 40657445-40679043, hg19) and 250,617 bases (chr2:40404996-40655612, hg19). We compared the intron sequences on both sides by BLAST (https://blast.ncbi.nlm.nih.gov/Blast.cgi) and found that there were a large of highly complementary sequences (Fig S1H). Such highly complementary sequences readily formed dimers, thereby promoting back-splicing to form circular RNAs (Fig 3K). This may be the reason for the high abundance of cSLC8A1 in RCC cells[14].

(iii) It has been reported that cSLC8A1 can inhibit the proliferation and metastasis of bladder cancer[15]. Although there is heterogeneity among different tumors, the tumor suppressor function of cSLC8A1 in tumors can provide us with a reference.

cSLC8A1 is associated with sunitinib resistance in RCC in vitro and in vivo

To thoroughly explore the function of cSLC8A1 in sunitinib resistance, we used lentiviral transduction to suppress cSLC8A1 expression in ACHN and 786-O cells. We used RT-PCR to detect the efficiency of sh-RNA transduction (Fig S2A). The IC50 and the cell colony formation capacity under the stimulation of sunitinib were increased in the sh-cSLC8A1 groups compared with the control groups (Fig 4A, B). Next, we overexpressed cSLC8A1 in Sun-7R and Sun-AR cells and evaluated the overexpression efficiency by RT-PCR (Fig S2B). Compared with the control groups, the oe-cSLC8A1 groups exhibited decreased IC50 values and cell colony formation capacity under the stimulation of sunitinib (Fig 4C, D). Then, we injected

786-O and sh-cSLC8A1 786-O cells subcutaneously into the axillae of nude mice. When the volume of the xenografts was 100 mm^3, the mice were treated orally with vehicle or sunitinib (40 mg/kg/day). The xenografts derived from sh-cSLC8A1 RCC cells exhibited worse responses to sunitinib (Fig 4E，Fig S2C). These findings indicate that suppression of cSLC8A1 can promote sunitinib resistance in RCC cell lines.

cSLC8A1 can competitively bind to the FUS protein and promote its ubiquitination and degradation

To verify whether cSLC8A1 has the function of binding proteins, we performed an RNA pulldown assay to identify the target protein and predict the binding site through the database. The cSLC8A1 pulldown product was analyzed by mass spectrometry, and a total of 92 proteins were found (Supplementary Data 4, Fig S2D). The top 10 proteins were selected using MaxQuant software (Fig 5A). Next, we analyzed the possible binding RBPs of cSLC8A1 through the Starbase database (http://starbase.sysu.edu.cn/) and the IDCSC (International Database Cancer-Special circRNA) database (http://geneyun.net/IDCSC/). We ranked these proteins according to the number of predicted binding sites (Fig S2E, Supplementary Data 5). Combining these findings with bioinformatic data, we selected FUS as the target protein for further research. In order to verify cSLC8A1 whether could bind to FUS protein, we performed RNA immunoprecipitation (RIP) in RCC 786-O and ACHN cell lines using FUS antibodies. The qRT-PCR results showed that FUS can enrich cSLC8A1(Fig 5B,C). The result of RNA-protein immunofluorescence colocalization showed that cSLC8A1 and FUS were colocalized in the cytoplasm and nucleus (Fig 5D). The above results indicate that cSLC8A1 can directly bind to FUS protein. Then, we detected the expression of FUS in RCC cell lines. The levels of FUS expression in sh-cSLC8A1 786-O and ACHN cell lines were increased compared with those in the corresponding control cells; however, the FUS expression levels in the oe-SLC8A1 cell lines were significantly lower than those in Sun-7R and Sun-AR cell lines (Fig 5E, F). The RT-PCR results showed no significant changes in the mRNA level of FUS after modulating the expression of cSLC8A1 (Fig S2F). These results indicated some intrinsic relationship between cSLC8A1 and FUS proteins, rather than FUS mRNA.

The results in RCC cell lines and patient tissues were consistent. The expression level of FUS protein in sunitinib-resistant cells and tissues increased, but the qRT-PCR results showed no significant difference in the mRNA expression of FUS (Fig 5G, H, Fig S2G). We prepared tissue microarrays from 133 patients before treated with sunitinib and performed immunohistochemistry (IHC). Patients were divided into sunitinib-sensitive groups （n=99）and sunitinib-resistant groups（n=33）based on their benefit from sunitinib treatment (Table2). According to the H-score of IHC, we found that the expression of FUS in the sunitinib-resistant groups was higher than that in the sensitive groups (Fig 5I). The correlation analysis of cSLC8A1 expression level and FUS protein expression in tumor tissues of 46 RCC patients showed that cSLC8A1 expression was inversely related to the expression of FUS (Fig 5J). To further explore the mechanism by which cSLC8A1 affects the level of the FUS protein, we performed a cycloheximide (CHX) chase assay. The results of this assay demonstrated that overexpression of cSLC8A1 decreased the stability of FUS (Fig 5K). Ubiquitination-mediated degradation is an important way mechanism for of FUS

degradation. We verified the level of ubiquitination in the over-expressing cSLC8A1cSLC8A1-overexpressing and normal parental 786-O cells line. Through immunoprecipitation (IP), we found that FUS protein the ubiquitination of FUS protein was significantly increased in the oe-cSLC8A1 786-O cells lines compared to the corresponding control group cells (Fig 5L). Related results indicated that cSLC8A1 binds to the FUS protein, promotes FUS its ubiquitination, reduces FUS its stability, and accelerates FUS protein its degradation.

Knockdown of FUS reverses the effect of cSLC8A1 on sunitinib resistance

We used lentiviral transduction to knock down FUS expression (Fig S2H). We found that the IC50 and the cell colony formation capacity were decreased in sh-FUS Sun-7R and Sun-AR cells compared with the corresponding control cells (Fig 6A, B). Transwell migration and invasion assays indicated that the migration and invasion abilities of Sun-7R and Sun-AR cells were also suppressed by knockdown of FUS (Fig 6C). The wound healing assay revealed that knockdown of FUS significantly inhibited cell migration in Sun-7R and Sun-AR cells (Fig 6D). “Rescue” experiments were performed, and the results showed that inhibiting FUS eliminated the discrepancy in sunitinib sensitivity between the sh-cSLC8A1 cell line and the corresponding control RCC cell line and that overexpressing FUS reversed the effect of oe-cSLC8A1 in this RCC cell line (Fig 6E). These results were consistent with animal drug simulation experiments in vitro (Fig 6F). We next analyzed the correlation between FUS expression and progression-free survival (PFS) and over survival (OS) in clear cell renal cell carcinoma (ccRCC) patients treated with sunitinib and found that the therapeutic efficacy was lower in patients with high FUS expression (Fig 6G). Multivariate Cox regression analysis showed that FUS were independent risk factors for a poor response to sunitinib treatment (Fig 6H, Table S3). These results indicate that cSLC8A1 promotes sunitinib resistance through FUS.

Low cSLC8A1 levels predict a poor response to sunitinib in RCC patients

As cSLC8A1 was functionally involved in the response to sunitinib in RCC cells, we further evaluated whether the expression of cSLC8A1 in tumor tissues was associated with the response to sunitinib therapy. We measured cSLC8A1 levels in RCC patient tissues. We divided patients into a high expression group and a low expression group according to the expression of cSLC8A1, and we found that patients with low expression of cSLC8A1 had shorter PFS and OS times than patients with high expression (Fig 7A, B). Through multivariate Cox regression analysis, we found that high Fuhrman grade and low expression of cSLC8A1 were independent risk factors for a poor response to sunitinib treatment (Fig 7C, Table S2). In addition, analysis of correlations between cSLC8A1 expression and clinicopathologic features indicated that the expression of cSLC8A1 was negatively associated with preoperative metastasis (Table 1).

Discussion

Kolakovsky and Sanger first discovered circRNAs in Sendai virus and plant-infecting viroids in 1976[16, 17]. CircRNAs are a new class of RNAs generated by pre-mRNA backsplicing, and many are highly stable and abundantly expressed in cells and tissues. Owing to their circular structure, circRNAs have higher stability to exist in the human nuclei and avoid degradation by RNases[12]. Initially, circRNAs were considered nonfunctional. However, with the development of RNA-Seq and bioinformatics approaches, an increasing number of functions of circRNAs have been found. CircRNAs function through various mechanisms, including (1) acting as miRNA sponges, (2) binding to many RNA-binding proteins and regulating protein functions, and (3) serving as protein scaffolds[18]. Many studies have proved that circRNAs were involved in important physiological processes of tumorigenesis and development, and were closely related to tumor proliferation, invasion, and metastasis. Huang W et al found that circAF4 can regulate MLL-AF4 fusion protein expression and act as a miR-168-3p sponge to inhibit MLL leukemia[19]. cSMARCA5 inhibits the growth and metastasis of HCC through the miR-17-3p/miR-181b-5p-TIMP3 pathway[20]. In RCC, Circ-AKT3 inhibits clear cell renal cell carcinoma metastasis via altering miR-296-3p/E-cadherin signals[8]. Our previous research also found that cRAPGEF5 inhibits the growth and metastasis of renal cell carcinoma via the miR-27a-3p/TXNIP pathway[21]. All previous studies on circRNAs in RCC focused on metastasis, and until this study, no studies had addressed the mechanism of circRNA in targeted drug resistance in RCC[22].

In this study, we generated sunitinib-resistant RCC cell lines, Sun-7R and Sun-AR, and we then we identified the differentially expressed circRNAs between Sun-7R and 786-O cells by RNA-Seq. We were the first to report the expression profile of circRNAs in targeted drug resistance of RCC. Our sequencing results showed that circRNAs were mainly low-expressed in sunitinib-resistant RCC cell lines. This result is similar to that of Josh et al., who suggested that cellular proliferation in tumor tissue may lead to the downregulation of circRNAs, a mechanism also proposed by Bachmayr-Heyda et al[23, 24]. We found that cSLC8A1 was high abundance and significantly downregulated in sunitinib resistance cells and tissues. cSLC8A1 consists of a 1832 bp exon of the slc8a1 gene, and was a high-abundance expression in cardiomyocytes[25]. cSLC8A1 plays an important role in many diseases, such as cancers, Parkinson's disease and cardionmyocytes[26–28]. For instance, cSLC8A1 is downregulated in bladder cancer and acts as a sponge of miR-130b/miR-494[15]. In addition, cSLC8A1 also can sponge miR-671 to regulate breast cancer tumorigenesis via the PTEN/PI3k /Akt pathway[29]. In our study cSLC8A1 also exhibited an inhibitory effect on tumor progression.

The mechanisms of circRNAs are diverse, and most research had focused on its role as a miRNA sponge. CircRNAs possess conserved protein-binding sequences, which can act as protein scaffolds to facilitate the connection between proteins[30]. We found a novel function of cSLC8A1, which was that it regulates the expression level of proteins after directly binding to RBP. Yang et al. found that circAmotl1 was significantly upregulated in breast cancer, and that circAmotl1 and c-myc co-localized in the nucleus[31]. The combination of circAmotl1 and c-myc can induce the transfer of c-myc out of the nucleus, and also

inhibit the degradation of c-myc and promote tumorigenesis. In this study, we used mass spectrometry and database to analyze the target protein of cSLC8A1, and we found that the FUS protein could bind cSLC8A1 directly. FUS was originally identified as a fusion protein that resulted from a chromosomal translocation in human myxoid liposarcomas[32]. As an RNA-binding protein, FUS has the advantage of competitively binding to circular RNAs[33]. Previous studies have shown that both FUS protein and mSLC8A1 are localized in the nucleus[34]. What is interested we found that cSLC8A1 binds to FUS protein in the cytoplasm in our study. Whether nuclear translocation occurs after cSLC8A1 binds to FUS and affects biological function is worthy of our further study. FUS could regulate transcription and DNA damage, and then in turn regulate cellular function processes, including proliferation, apoptosis, invasion, migration and angiogenesis[33, 35, 36]. Liu et. al found that FUS could induce circ-ZNF609 expression and promote the progression of lung cancer[37]. We found FUS was key protein which promoted drug resistance in RCC. The SLC8A1 p-mRNA was back-spliced to form a circular RNA, which was combined with FUS and promoted ubiquitination, and accelerates FUS proteinits degradation. In our study, FUS protein was an oncogene, which could promote sunitinib resistance in RCC.

Conclusion

We explored the role and mechanism of circRNAs in sunitinib resistance in RCC for the first time and identified a resistance-related circular RNA, cSLC8A1. The results showed that cSLC8A1 can inhibit resistance by promoting the ubiquitination and degradation of the FUS protein. Multivariate Cox regression analysis showed that cSLC8A1 can be used as an independent factor for predicting the efficacy of sunitinib in RCC. Therefore, cSLC8A1 plays an important role in drug resistance and is expected to become a target for reversing sunitinib resistance in RCC. Although targeted drugs and immune checkpoint inhibitors are currently two important methods for the treatment of advanced RCC, TKI drugs are still the first-line treatment. In the future, we will focus on circRNAs change the immune microenvironment to promote the efficacy of targeted therapy.

Abbreviations

TKI: Tyrosine Kinase Inhibitor; RBP: RNA-binding protein; FBS: fetal bovine serum; FUS: fused in sarcoma; RIP: RNA Binding Protein Immunoprecipitation; Co-IP: Co-immunoprecipitation; VEGF: vascular endothelial growth factor.

Declarations

Ethics approval and consent to participate

The research protocol was reviewed and approved by the ethics committee of Changzheng Hospital Affiliated with Naval Military Medical University and Changhai Hospital Affiliated with Naval Military Medical University. Written informed consent was obtained from each patient included in the study.

Consent for publication

Not applicable.

Availability of data and materials

Please contact the corresponding author for all data requests.

Competing interests

The authors declare that they have no competing interests

Funding

The study was supported by the National Natural Science Foundation of China (81730073,81872074,82072818) and the Clinical Science and Technology Innovation Project of Shanghai Shenkang Hospital Development Center (SHDC12021118).

Authors' contributions

Wang LH and Wang J conceived and designed the experiments. Wang YX and Yang F improved the experiment design. Wang J, Gan XX and Chen Q carried out major part of the project and analyzed of data. Liu B and Zheng SJ wrote the manuscript. Bao Y and Wang AB collect the clinical data. Yan R, Bao YW and Gong WL analyzed the clinical data and wrote a part of manuscript. All authors read and approved the final manuscript.

Acknowledgments

Not applicable.

References

1. Siegel R L, Miller K D, Fuchs H E, et al. Cancer Statistics, 2021[J]. CA Cancer J Clin, 2021,71(1):7-33.
2. Ljungberg B, Bensalah K, Canfield S, et al. EAU guidelines on renal cell carcinoma: 2014 update[J]. Eur Urol, 2015,67(5):913-924.
3. Hsieh J J, Purdue M P, Signoretti S, et al. Renal cell carcinoma[J]. Nat Rev Dis Primers, 2017,3:17009.
4. Barata P C, Rini B I. Treatment of renal cell carcinoma: Current status and future directions[J]. CA Cancer J Clin, 2017,67(6):507-524.

5. Choueiri T K, Motzer R J. Systemic Therapy for Metastatic Renal-Cell Carcinoma[J]. N Engl J Med, 2017,376(4):354-366.
6. Powles T, Staehler M, Ljungberg B, et al. Updated EAU Guidelines for Clear Cell Renal Cancer Patients Who Fail VEGF Targeted Therapy[J]. Eur Urol, 2016,69(1):4-6.
7. Kristensen L S, Andersen M S, Stagsted L, et al. The biogenesis, biology and characterization of circular RNAs[J]. Nat Rev Genet, 2019,20(11):675-691.
8. Xue D, Wang H, Chen Y, et al. Circ-AKT3 inhibits clear cell renal cell carcinoma metastasis via altering miR-296-3p/E-cadherin signals[J]. Molecular Cancer, 2019,18(1):151.
9. Ma S, Kong S, Wang F, et al. CircRNAs: biogenesis, functions, and role in drug-resistant Tumours[J]. Mol Cancer, 2020,19(1):119.
10. Zhou R, Wu Y, Wang W, et al. Circular RNAs (circRNAs) in cancer[J]. Cancer Letters, 2018,425:134-142.
11. Chen S, Huang V, Xu X, et al. Widespread and Functional RNA Circularization in Localized Prostate Cancer[J]. Cell, 2019,176(4):831-843.
12. Su M, Xiao Y, Ma J, et al. Circular RNAs in Cancer: emerging functions in hallmarks, stemness, resistance and roles as potential biomarkers[J]. Molecular cancer, 2019,18(1):90.
13. Miao D, Margolis C A, Gao W, et al. Genomic correlates of response to immune checkpoint therapies in clear cell renal cell carcinoma[J]. Science, 2018,359(6377):801-806.
14. Zhang X O, Wang H B, Zhang Y, et al. Complementary sequence-mediated exon circularization[J]. Cell, 2014,159(1):134-147.
15. Lu Q, Liu T, Feng H, et al. Circular RNA circSLC8A1 acts as a sponge of miR-130b/miR-494 in suppressing bladder cancer progression via regulating PTEN[J]. Mol Cancer, 2019,18(1):111.
16. Kolakofsky D. Isolation and characterization of Sendai virus DI-RNAs[J]. Cell, 1976,8(4):547-555.
17. Sanger H L, Klotz G, Riesner D, et al. Viroids are single-stranded covalently closed circular RNA molecules existing as highly base-paired rod-like structures[J]. Proc Natl Acad Sci U S A, 1976,73(11):3852-3856.
18. Wilusz J E. A 360 degrees view of circular RNAs: From biogenesis to functions[J]. Wiley Interdiscip Rev RNA, 2018,9(4):e1478.
19. Huang W, Fang K, Chen T Q, et al. circRNA circAF4 functions as an oncogene to regulate MLL-AF4 fusion protein expression and inhibit MLL leukemia progression[J]. J Hematol Oncol, 2019,12(1):103.
20. Yu J, Xu Q G, Wang Z G, et al. Circular RNA cSMARCA5 inhibits growth and metastasis in hepatocellular carcinoma[J]. J Hepatol, 2018,68(6):1214-1227.
21. Chen Q, Liu T, Bao Y, et al. CircRNA cRAPGEF5 inhibits the growth and metastasis of renal cell carcinoma via the miR-27a-3p/TXNIP pathway[J]. Cancer Lett, 2020,469:68-77.
22. Wang Y, Zhang Y, Wang P, et al. Circular RNAs in renal cell carcinoma: implications for tumorigenesis, diagnosis, and therapy[J]. Mol Cancer, 2020,19(1):149.

23. Vo J N, Cieslik M, Zhang Y, et al. The Landscape of Circular RNA in Cancer[J]. Cell, 2019,176(4):869-881.
24. Bachmayr-Heyda A, Reiner A T, Auer K, et al. Correlation of circular RNA abundance with proliferation--exemplified with colorectal and ovarian cancer, idiopathic lung fibrosis, and normal human tissues[J]. Sci Rep, 2015,5:8057.
25. Tan W L, Lim B T, Anene-Nzelu C G, et al. A landscape of circular RNA expression in the human heart[J]. Cardiovasc Res, 2017,113(3):298-309.
26. Lim T B, Aliwarga E, Luu T, et al. Targeting the highly abundant circular RNA circSlc8a1 in cardiomyocytes attenuates pressure overload induced hypertrophy[J]. Cardiovasc Res, 2019,115(14):1998-2007.
27. Hanan M, Simchovitz A, Yayon N, et al. A Parkinson's disease CircRNAs Resource reveals a link between circSLC8A1 and oxidative stress[J]. EMBO Mol Med, 2020,12(9):e11942.
28. Zhu J, Liu X, Luan Z, et al. Circular RNA circSLC8A1 inhibits the proliferation and invasion of glioma cells through targeting the miR-214-5p/CDC27 axis[J]. Metab Brain Dis, 2022.
29. Zhu Q, Zhang X, Zai H Y, et al. circSLC8A1 sponges miR-671 to regulate breast cancer tumorigenesis via PTEN/PI3k/Akt pathway[J]. Genomics, 2021,113(1 Pt 1):398-410.
30. Zhu Y, Zheng B, Luo G, et al. Circular RNAs negatively regulate cancer stem cells by physically binding FMRP against CCAR1 complex in hepatocellular carcinoma[J]. Theranostics, 2019,9(12):3526-3540.
31. Yang Q, Du WW, Wu N, et al. A circular RNA promotes tumorigenesis by inducing c-myc nuclear translocation[J]. Cell Death Differ, 2017,24(9):1609-1620.
32. Patel A, Lee H O, Jawerth L, et al. A Liquid-to-Solid Phase Transition of the ALS Protein FUS Accelerated by Disease Mutation[J]. Cell, 2015,162(5):1066-1077.
33. Errichelli L, Dini M S, Laneve P, et al. FUS affects circular RNA expression in murine embryonic stem cell-derived motor neurons[J]. Nat Commun, 2017,8:14741.
34. Hofweber M, Hutten S, Bourgeois B, et al. Phase Separation of FUS Is Suppressed by Its Nuclear Import Receptor and Arginine Methylation[J]. Cell, 2018,173(3):706-719.
35. Garikipati V, Verma S K, Cheng Z, et al. Circular RNA CircFndc3b modulates cardiac repair after myocardial infarction via FUS/VEGF-A axis[J]. Nat Commun, 2019,10(1):4317.
36. Sato S, Idogawa M, Honda K, et al. Beta-catenin interacts with the FUS proto-oncogene product and regulates pre-mRNA splicing[J]. Gastroenterology, 2005,129(4):1225-1236.
37. Liu S, Yang N, Jiang X, et al. FUS-induced circular RNA ZNF609 promotes tumorigenesis and progression via sponging miR-142-3p in lung cancer[J]. J Cell Physiol, 2021,236(1):79-92.

Tables

Table 1

Clinical characteristics of 46 RCC patients according to cSLC8A1 expression level

Variables	Low cSLC8A1 (n=23)	High cSLC8A1 (n=23)	P-value
Gender			0.502
Male	18	16	
Female	5	7	
Age			0.76
≤60y	14	15	
60y	9	8	
Tumor size			0.522
≤7*cm*	8	6	
7*cm*	15	17	
Fuhrman grade			0.139
I/II	10	15	
III/IV	13	8	
Tumor thrombus			0.753
Yes	8	7	
No	15	16	
Lymph node metastasis			0.722
Yes	4	6	
No	19	17	
Metastasis pre-operative			**0.038***
Yes	14	7	
No	9	16	
TNM stage			0.314
I/II	4	8	
III/IV	19	15	

Table 2

Clinical characteristics of 133 RCC patients according to FUS expression level in IHC

Variables	Low FUS (n=67)	High FUS (n=66)	P-value
Gender			0.3
Male	52	46	
Female	15	20	
Age			0.546
≤60y	37	33	
60y	30	33	
Tumor size			0.641
≤7*cm*	27	24	
7*cm*	40	42	
Fuhrman grade			0.784
I/II	37	38	
III/IV	30	28	
Tumor thrombus			0.183
Yes	32	24	
No	35	42	
Lymph node metastasis			0.479
Yes	11	8	
No	56	58	
Metastasis pre-operative			**0.001***
Yes	17	36	
No	50	30	
TNM stage			0.351
I/II	20	15	
III/IV	47	51	

Figures

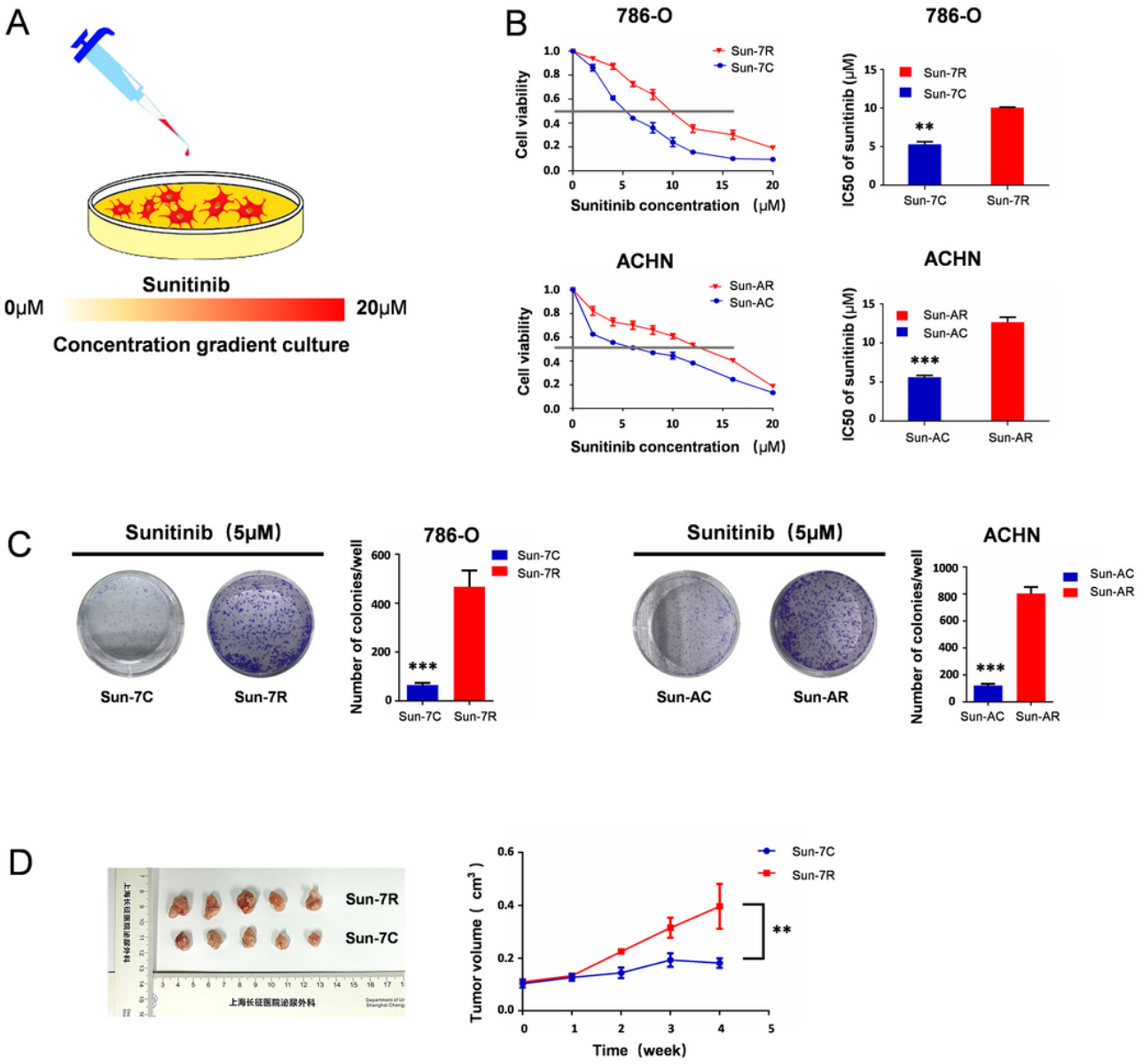

Figure 1

Figure 1

Successful construction of sunitinib-resistant cell line for RCC

A. Schematic diagram of the method for constructing sunitinib-resistant cell lines in RCC. **B.**CCK-8 assay of Sun-7R and Sun-AR cells and their parental control cells after treatment with sunitinib at concentrations of 0-20 μM for 48 h. **C.** Plate colony formation assay of Sun-7R and Sun-AR with their parental control cells after sunitinib treatment (5 μM) **D.** Hypodermic injection of 786-O and Sun-7R cells subcutaneously into the axillae of nude mice. The mice were treated orally with sunitinib (40 mg/kg/day). Growth curve of subcutaneous xenografts showed the tumor of Sun-7R was worse responses to sunitinib. Data are mean ± SD, n = 3, * p<0.05, ** p<0.01,***p<0.001.

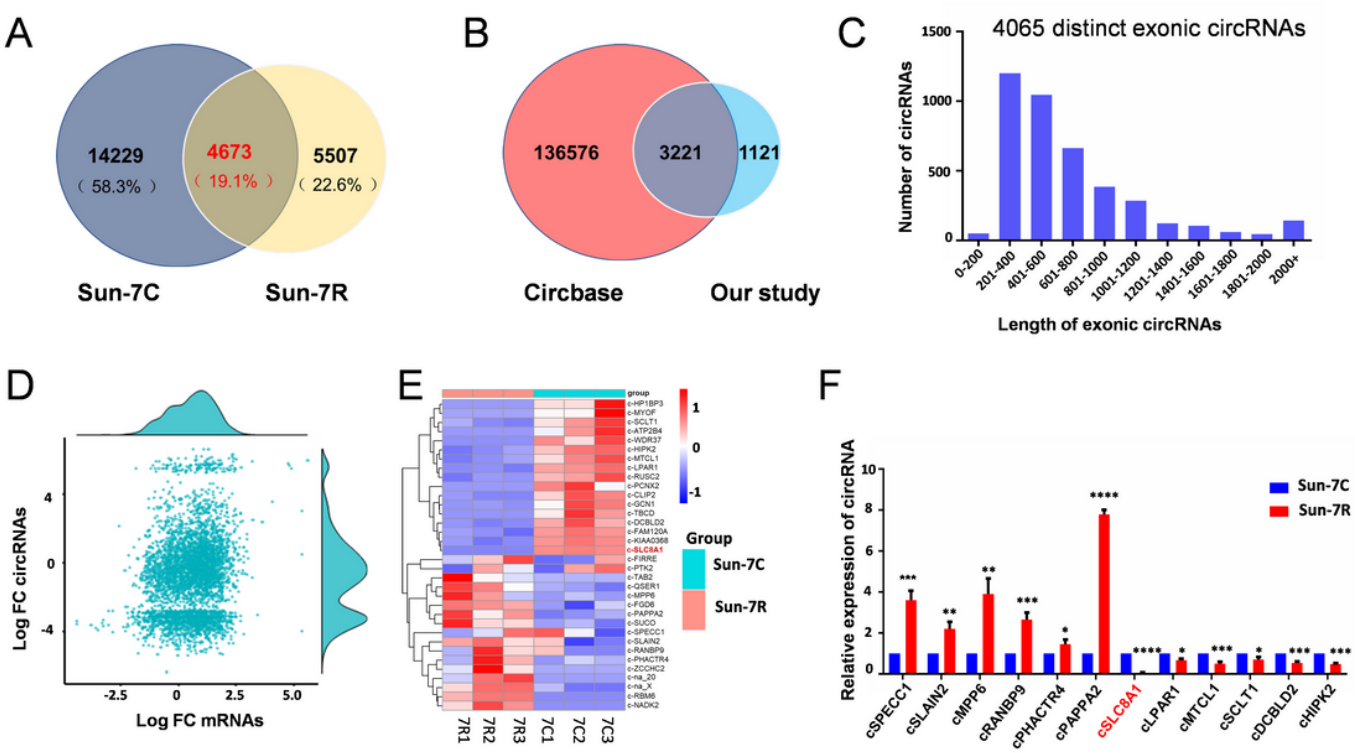

Figure 2

Figure 2

Identification of circular RNAs by RNA-seq analyses in sunitinib-resistant RCC cells.

A. Venn diagram showing the distributions of total circRNAs between Sun-7R and Sun-7C cells as determined by RNA-HiSeq. **B.** Most of the circRNAs identified in our study overlapped with circBase. **C.** The length distribution of circRNAs formed by exons showed that most of their length were less than 1000 bases. **D.** Correlation of fold-change in abundance of each circRNA (Y axis) and its cognate mRNA (X axis) between resistant cell and control cell. The individual distribution profiles of each are shown above and to the right of the correlation plot. The distributions of cognate mRNA showed normal distribution, but there were three peaks in circRNAs distribution. **E.** Cluster heat map of the significantly differentially expressed circRNAs in Sun-7R and Sun-7C cells. **F.** qRT-PCR was used to verify the expression of 12 circRNAs in Sun-7R cells and Sun-7C cells. Data are mean ± SD, n = 3, * $p<0.05$, ** $p<0.01$, ***$p<0.001$, ****$p<0.0001$.

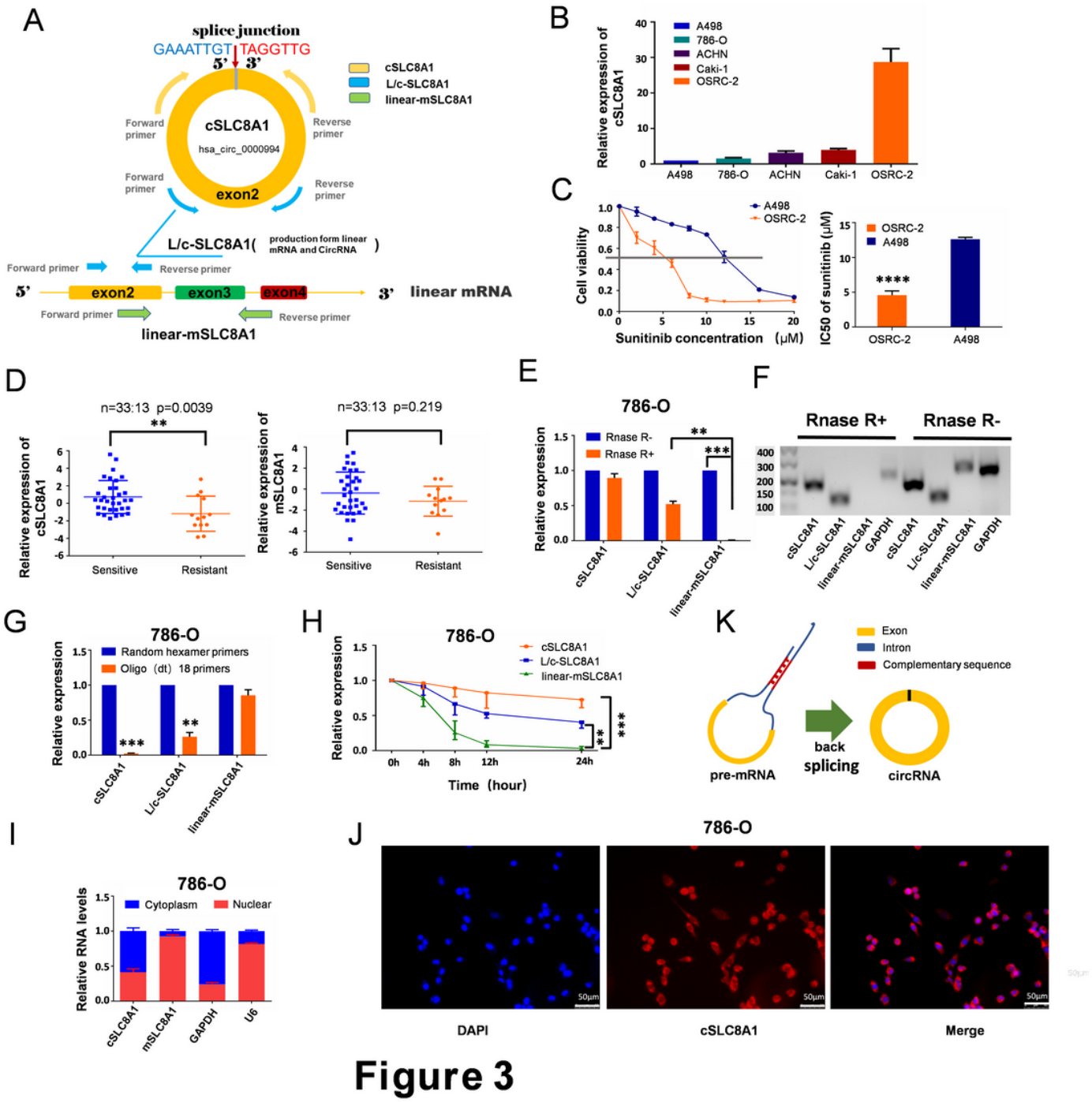

Figure 3

Figure 3

The characteristics of the circular RNA cSLC8A1.

A. Schematic illustration showing the circularization of circSLC8A1. Three different primers were designed based on their structural characteristics. cSLC8A1: Circular RNA-specific primer, the product was from cSLC8A1; linear-mSLC8A1: linear mRNA -specific primer, the product was from linear-mSLC8A1; L/c-SLC8A1:SLC8A1 public primer, the product was from linear-mSLC8A1 and cSLC8A1. Red arrow indicates

the special splicing junction of cSLC8A1. **B.** The expression of cSLC8A1 in different RCC cell lines. **C.** The concentration-response curves and IC50 showed the A498 RCC cell was more resistant to sunitinib when its cSLC8A1 expression lower compared with OSRC-2 RCC cell. **D.** The expression of cSLC8A1 and mSLC8A1 in pretherapy tumor tissues of RCC patients with poor responses (n=13) and good responses (n=33) to sunitinib therapy. **E.** The relative RNA levels were analyzed by qRT-PCR before and after RNase R treatment. **F.** The products were identified by agarose gel electrophoresis. **G.** qRT-PCR results of the amplification products after reverse transcription of cDNA with random primers and oligo(dT)18 primers. **H.** The relative RNA levels of cSLC8A1, linear mSLC8A1 and L/c-SLC8A1 were determined by qRT-PCR after treatment with actinomycin D (2 μg/ml) at different time points. **I.** The proportions of each molecule in the nuclear and cytoplasmic fractions were determined by qRT-PCR. **J.** The results of FISH showed that the subcellular localization of cSLC8A1 could be either the nucleus or the cytoplasm. Blue fluorescence, DAPI; red fluorescence, cSLC8A1. K. Highly reverse complementary sequences easily form dimers, which facilitates reverse splicing to form circular RNA. Data are mean ± SD, n = 3, * $p<0.05$, ** $p<0.01$, ***$p<0.001$, ****$p<0.0001$.

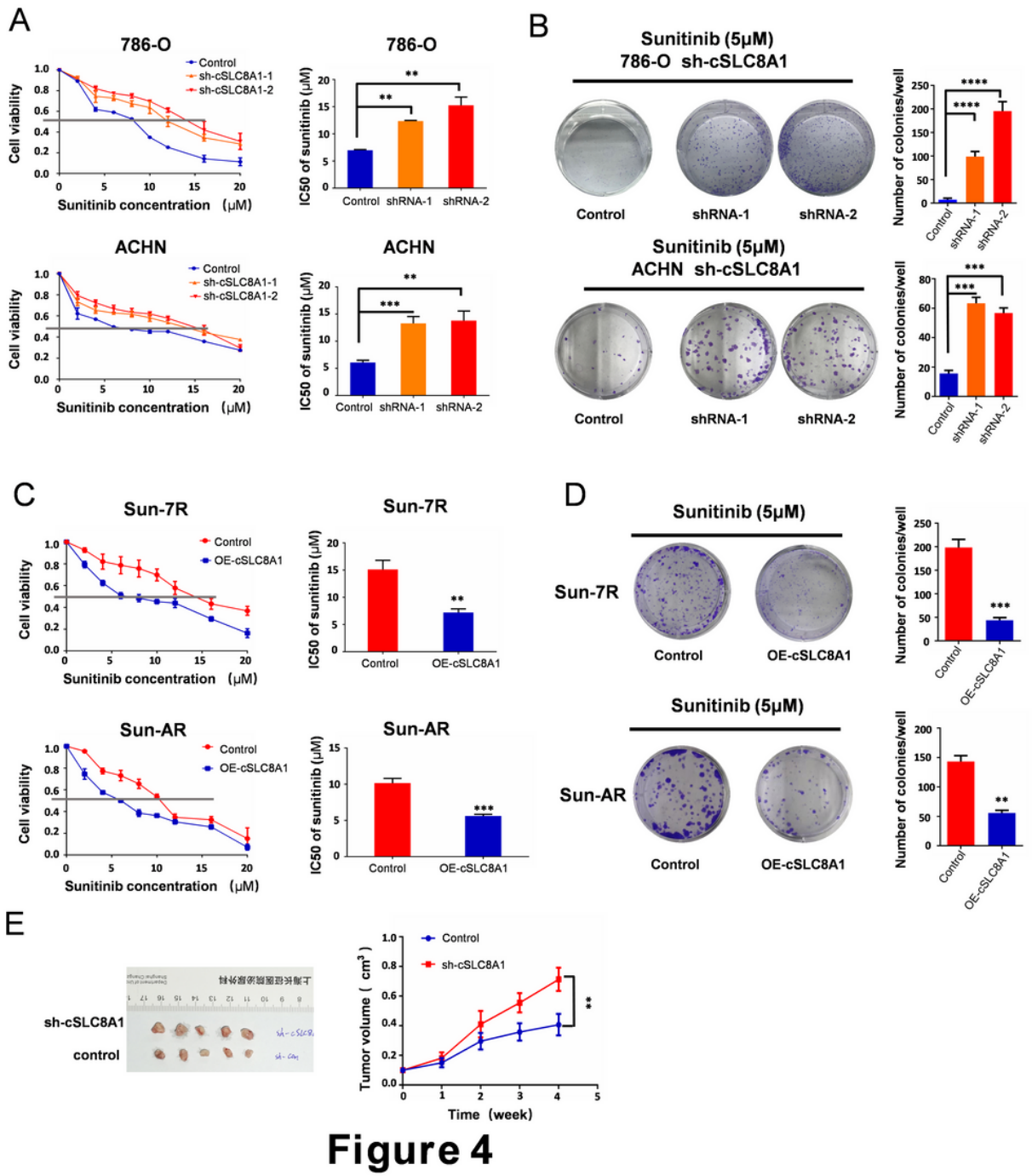

Figure 4

Figure 4

cSLC8A1 enhances the sensitivity of cell lines to sunitinib.

A&C. CCK-8 assays of 786-O and ACHN cells with cSLC8A1 knockdown and overexpression compared with the corresponding parental control cells after treatment with 0-20 μM sunitinib for 48 h. **B&D**. Plate colony formation assay of 786-O and ACHN cells with cSLC8A1 knockdown and overexpression compared with the corresponding parental control cells after sunitinib treatment (5 μM). **E.** Hypodermic injection of 786-O cells stably transfected with Lv-sh-cSLC8A1 or control vector subcutaneously into the axillae of nude mice. The mice were treated orally with sunitinib (40 mg/kg/day). Growth curve of

subcutaneous xenografts showed the tumor was resistant to sunitinib after cSLC8A1 knockdown. Data are mean ± SD, n = 3, * p<0.05, ** p<0.01, ***p<0.001, ****p<0.0001.

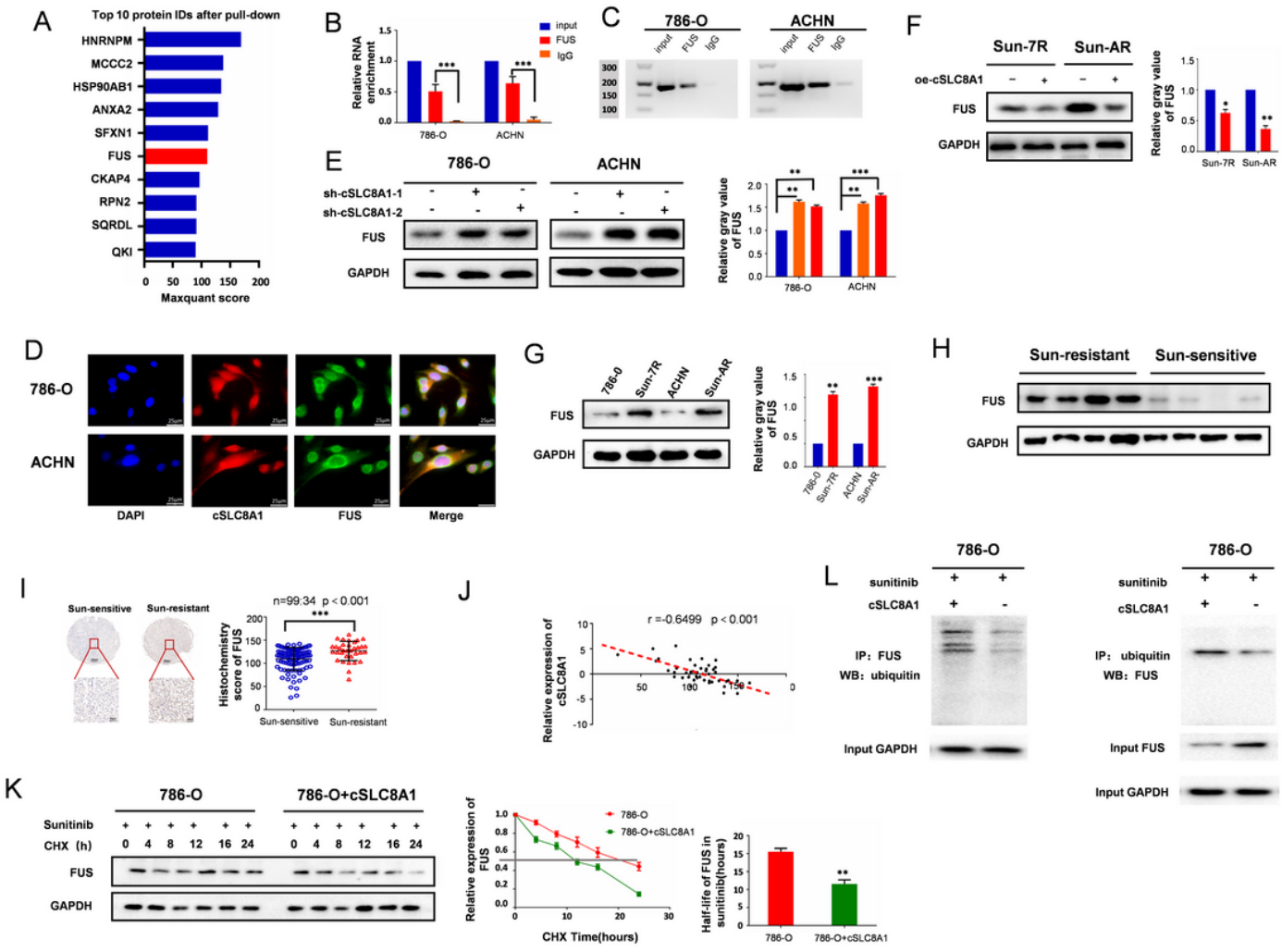

Figure 5

Figure 5

cSLC8A1 can competitively bind to the FUS protein and promote its ubiquitination and degradation.

A. The top 10 proteins by cSLC8A1 Pull-down protein mass spectrometry ranked according to the MaxQuant software score. **B.** RIP was performed in RCC 786-O and ACHN cell lines using an anti-FUS antibody. The qRT-PCR results showed that FUS can enrich cSLC8A1. **C.** The results of agarose electrophoresis showed that FUS can enrich cSLC8A1. D. Co-localization between cSLC8A1 and FUS was observed by RNA-protein immunofluorescence in 786-O and ACHN. Blue fluorescence, DAPI; red fluorescence, cSLC8A1; green fluorescence, FUS. **E.** Western blot was used to determine the protein level of FUS in 786-O and ACHN with cSLC8A1 knockdown. **F.** Western blot was used to determine the protein

level of FUS in Sun-7R and Sun-AR with cSLC8A1 overexpression. **G.** Western blot results showed that Sunitinib-resistant cell lines Sun-7R and Sun-AR had increased expression of FUS protein than their control normal cells. **H.** Western Blot was used to determine the protein level of FUS in the patients with sensitivity and resistance to sunitinib. **I.** Representative immunohistochemical results of FUS in tumor tissues of patients with sensitivity and resistance to sunitinib. **J.** Correlation analysis of cSLC8A1 expression and FUS protein expression levels in tumor tissues of 46 renal cancer patients. **K.** Western Blot verified the expression of FUS protein at different time points in the RCC 786-O control group and the overexpressing cSLC8A1 group under CHX (20 μg / ml) treatment. Protein inhibition -time curve showed faster degradation of FUS protein under CHX after overexpression of cSLC8A1. **L.** Evaluation of the ubiquitination level after overexpression of cSLC8A1. FUS antibody was co-immunoprecipitated and Western Blot was used to detect ubiquitinated protein. Ubiquitin antibody was co-immunoprecipitated and Western Blot was used to detect FUS protein. Data are mean ± SD, n = 3, * p<0.05, ** p<0.01, ***p<0.001.

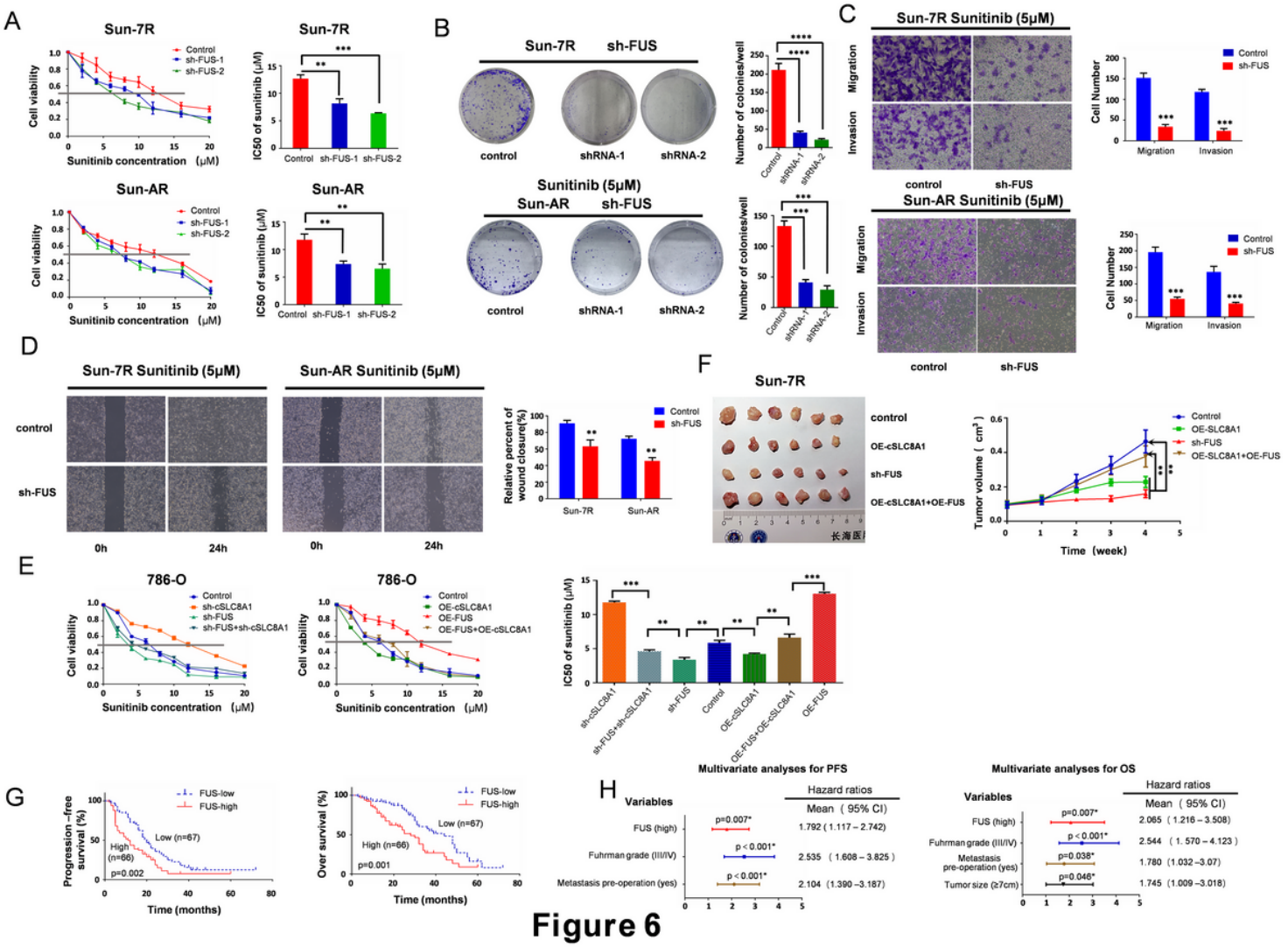

Figure 6

Figure 6

Knockdown of FUS restored sensitivity to sunitinib in sunitinib-resistant RCC cells. A. CCK-8 assay of Sun-7R and Sun-AR cell lines with FUS knockdown after treatment with 0-20 μM sunitinib for 48 h. **B.** Plate colony formation assay of Sun-7R and Sun-AR cell lines with FUS knockdown after sunitinib treatment (5 μM). **C.** Transwell migration and invasion assays indicated that the migration and invasion abilities of Sun-7R and Sun-AR cells with FUS knockdown after sunitinib treatment (5 μM) were suppressed. **D.** The effect of cell migration capability was evaluated by wound healing assay in Sun-7R and Sun-AR cell lines with FUS knockdown after sunitinib treatment (5 μM). **E.** "Rescue" experiments were performed by CCK-8 assay, and the results showed that inhibiting FUS eliminated the discrepancy in sunitinib sensitivity between the sh-cSLC8A1 cell line and the corresponding control RCC cell line and that overexpressing FUS reversed the effect of oe-cSLC8A1 in this RCC cell line. **F.** "Rescue" experiments were performed by animal drug simulation experiments in vitro. **H.** Kaplan–Meier analysis showed that patients with lower FUS expression had longer PFS and overall survival (OS) times. **I.** Multivariate analysis of hazard ratios for PFS and OS. Data are mean ± SD, n = 3, * p<0.05, ** p<0.01, ***p<0.001, ****p<0.0001.

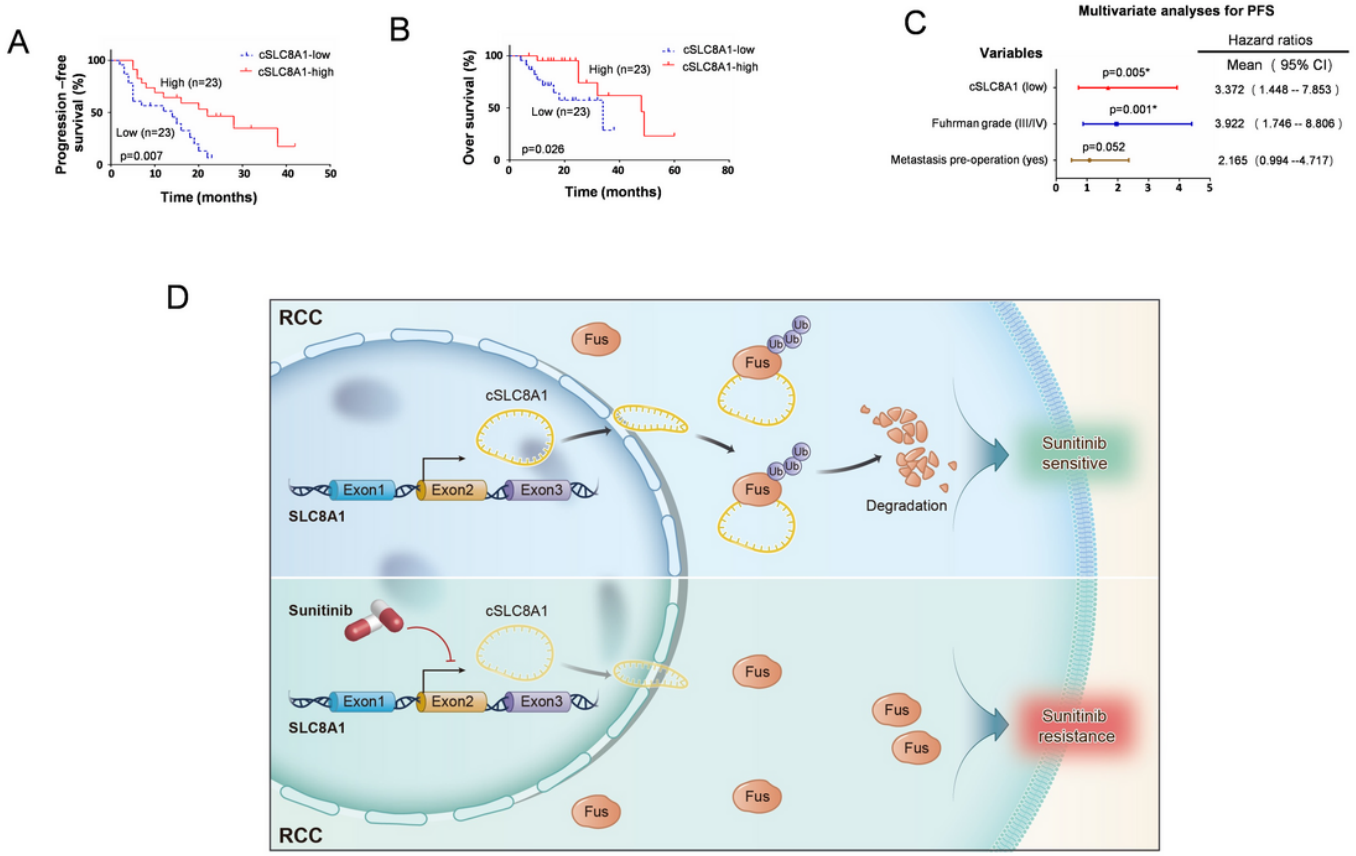

Figure 7

Figure 7

The relationship between cSLC8A1 and patients survival.

A&B. Kaplan–Meier analysis of PFS and OS in RCC patients stratified by cSLC8A1 expression. **C.** Multivariate analysis of hazard ratios for PFS.**D.** Mechanism graph of cSLC8A1 in sunitinib resistance in RCC. The SLC8A1 p-mRNA was back-spliced to form a circular RNA, which was combined with FUS and promoted FUS its ubiquitination, and accelerates FUS protein its degradation. FUS protein could promote sunitinib resistance in RCC.

Supplementary Files

This is a list of supplementary files associated with this preprint. Click to download.

- SupplementaryData1PrimersequencesforPCR.xlsx
- SupplementaryData2shRNAandnegativecontrolsequences.xlsx
- SupplementaryData335cirRNAs.xlsx
- SupplementaryData4massspectrometry.xlsx
- SupplementaryData5.xlsx
- SupplementaryFigure1.tif
- SupplementaryFigure2.tif
- TableS123.docx